19th Brazilian Congress of Thermal Sciences and Engineering
November 06th-10th, 2022, Bento Gonçalves - RS - Brazil

ENC-2022-0265

EFFECT OF NANOPARTICLE BIODISTRIBUTION IN THE LASER INDUCED THERMAL THERAPY: A SKIN CANCER EMBEDDED WITH GOLD NANOSHELLS

Ícaro Lucena
André Maurente
icarosjs@gmail.com
amaurente@gmail.com

Abstract. *The main objective of this study is to evaluate the effects caused by the variation of nanoparticles, after their deposition, in the tissue, verifying the possible changes in the heat flux and in the tissue temperature profile. A Skin cancer, diameter of 100 mm and thickness of 36 mm, with five layers (epidermis, tumor, papillary and reticular dermis and fat), for 10s, was irradiated by a helium-neon laser (laser power of 20 kW/m^2 and wavelength is 0.6328 μm). Slabs are one-dimensional and embedded with Silica-gold nanoshells (GNS) with following dimensions: r=10 nm (shell) and 0.725r (silica core), the volume fraction used was 10^{-5} particles. Numerical study used Monte Carlo and Finite volume approaches to solve the problem involving conduction, blood perfusion and radiation. Two spatial configurations are compared with uniform case: (I) GNS accumulated on epidermis and first half by the tissue and (II) GNS accumulated on tumor periphery. Case 1 produced a temperature profile sufficient to cause necrosis of cancerous tissues and mitigate damage to healthy areas, validated the importance of considering the position of nanoparticles as a key parameter in numerical studies, making it a probable variable, in the future, on in vivo, in vitro and clinical tests.*

Keywords: *GNS, biodistribution, Monte Carlo, Finite Volume, Skin.*

1. INTRODUCTION

Over the centuries, humanity has been joining efforts in the fight against cancer. Its incidence has been increasing progressively over time. “There were an estimated 19.3 million (95% uncertainty interval [UI]: 19.0-19.6 million) new cases of cancer (18.1 million excluding non-melanoma skin cancer) and almost 10.0 million (95% UI: 9.7-10.2 million) deaths from cancer (9.9 million excluding non-melanoma skin cancer) worldwide in 2020” (FERLAY et al. 2021).

Several treatments and studies are being developed in the search for greater effectiveness in fighting this disease, among them, the Photothermal Therapy (PTT), a category of hyperthermia, in which the affected tissue is overheated in order to kill diseased cells.

First report of hyperthermia in the history of modern medicine, according Januszewski and Stebbing (2014), occurred in 1898 when the gynecologist Frans Westermark used hot water in an intracavitary spiral tube for a local thermal response to a cervical carcinoma.

PTT can be used isolated or in conjunction with other treatments. “The use of hyperthermia alone has resulted in complete overall response rates of 13%. (VANDERZEE, 2002). “Generally, when combined with radiotherapy, no increase in radiation toxicity” (VANDERZEE, 2002).

One modality is laser-induced hyperthermia, which consists of irradiating small particles with a collimated infrared laser. Free electrons localized on a metallic nanoparticle surface are excited, according to Kim, Lee and Nam (2019), when this is illuminated by light causing variable asymmetric distribution on local electron clouds. This optical effect results on produces radiation absorption, consequently, changes in the temperature field.

According to Dombrovsky et al. (2011), three effects of hyperthermia detectable in the human body at a temperature above 42°C (42 to 50°C) are molecular changes, accompanied by bond destruction and membrane changes. These can also affect healthy tissues, so it is necessary to control some parameters to avoid healthy tissues and attain greater treatment efficiency. On the other hand, according to *Jain* et al. (2005), two conditions are fundamental to PTT, with a minimal laser dosage, effectiveness: high nanoparticle absorption cross-section and low scattering losses.

Metallic nanoparticles can be made up of various materials, (*e.g.*, gold, iron, silver) and shapes, (*e.g.*, rod, cage, shell). Many studies on numerical simulation with these particles are presented in the literature; two examples are gold nanoshells (DOMBROVSKY et al. 2011; SINGH, DAS, MISHRA, 2014) and gold nanorod (KIM. D., KANG, S., KIM, H, 2021). The biodistribution of these particles, in the vast majority of studies, is considered uniform.

Uniform distribution of particles on tissue, after the injection process, is unrealistic due to physical mechanisms. Many factors affect accumulation of nanoparticles: (a) Tumor physiology: vasculature morphology, pore size and interstitial fluid pressure; (b) Particle: size, shape, surface charge; (c) Injection parameters: rate, volume, concentration of the nanofluid; (d) Injection location: locally (around the injection site) and intravenous (around vascularized tumor region) (SONI and SINHA, 2016; SU et al. 2009)

An example of a numerical study evaluating the position of nanoparticles was carried out by Soni et al. (2014). They investigated the influence of gold nanorod (GNR) biodistribution on a bi-dimensional cylindrical skin cancer. The authors compared three cases: (I) Ideal case: GNR uniform distribution; (II) Intratumoral injection: GNR accumulated on tumor kernel; (III) Intravenous injection: GNR accumulated on tumor periphery. Using finite difference, energy balance and Monte Carlo methods to solve Pennes's bioheat and Beer-Lambert-Bouguer law equations. They conclude that nanoparticle deposition on tumor periphery, under controlled conditions, presents the most effective manner to realize the thermal therapy protocols.

The objective of this study is to understand the effects of nanoparticle biodistribution on the heat flux divergence and on the temperature profile with base on the temperature distribution of tumor and healthy tissues.

2. METHODOLOGY

The physical formulations and numerical methods are necessary to solve the studied problem of heat transfer in PTT are presented in this section. The procedure used in this study is like that performed by Bruno *et. a*l. 2017.

2.1 Heat Transfer fundamental equations and modeling

In photothermal therapy, there are three modes of heat transfer: conduction, blood perfusion and radiation. The first two heat transfer models are contemplated by the Pennes's bioheat equation (PBHE):

$$\rho c_p \frac{\partial T}{\partial t} = \nabla \cdot (k \nabla T) + \nabla \cdot q_r + \rho_b \upsilon_b c_b (T_b - T) \quad (1)$$

The problem analyzed is considered one-dimensional. Choosing the *z* direction for the analysis, the PBHE is reduced to:

$$\rho c_p \frac{\partial T}{\partial t} = \frac{d}{dz}\left(k \frac{dT}{dz}\right) + \frac{dq_{r,z}}{dz} + \rho_b \upsilon_b c_b (T_b - T) \quad (2)$$

In equations 1 and 2, ρ, k, c_p, T and t are, respectively, density, thermal conductivity, specific heat, tissue temperature; t is time, while; ρ_b, υ_b, c_b and T_b are, density, specific heat, perfusion rate and temperature of the blood. The subscript standing for blood. The last term was proposed by Pennes (1948) to compute the effects of blood perfusion. The second term after equality is the divergence of the radiative heat flux. It accounts for laser radiation absorption to obtains $q_{r,z}$ is necessary to solve the Radiative Transport Equation (RTE):

$$\frac{dI_\lambda}{dz} = \kappa_\lambda I_{b,\lambda} - \beta_\lambda I_\lambda + \frac{\sigma_{sc,\lambda}}{4\pi} \int_{\Omega_i=0}^{4\pi} \Phi_\lambda(\Omega, \Omega_i) I_{\lambda,i}(\Omega_i) d\Omega_i \quad (3)$$

where $I_{b,\lambda}$, I_λ, $I_{\lambda,i}$ are, respectively, blackbody spectral intensity (Planck function), variation of the intensity of radiation and variation of the incident intensity of radiation; κ_λ, $\sigma_{sc,\lambda}$, β_λ are the coefficients: absorption, scattering and extinction, respectively; Ω and Ω_i are direction to coordinates of the solid angle: propagation and incident, in order; $\Phi_\lambda(\Omega, \Omega_i)$ is the scattering phase function: account for the probability of a incoming ray from direction Ω_i scattering to direction Ω; The subscript λ indicates a relationship with the wavelength;

Emission of radiation from the tissue is negligence, because it is very low as compared to the laser power, scattering is assumed isotropic and radiation from laser is monochromatic, in this case, Eq. (3) reduces to

$$\frac{dI}{dz} = -\beta I + \frac{\sigma_{sc}}{4\pi} \int_{\Omega_i=0}^{4\pi} I_i(\Omega_i) d\Omega_i \quad (4)$$

Intensity, in Eq. (4), have two physics components: (1) Collimated: compute the effect of coming radiation directly from a laser; (2) Diffuse: compute the effect of scattering. To reduce this problem, a source term, S_c, Eq. (6), as presented by Modest (2003) is:

$$\frac{dI}{dz} = -\beta I + \frac{\sigma_{sc}}{4\pi} \int_{\Omega_i=0}^{4\pi} I_i(\Omega_i) d\Omega_i + S_c \quad (5)$$

Where

$$S_c = q_0 \frac{1}{4\pi}(1 - R_e) exp\,(-\int_0^z \beta dz^*) \quad (6)$$

In the above equation, z denotes the depth into the tissue from the surface where the radiation insides; q_0 is the laser power; R_e is the reflectivity of external surface, subscript e, to slab irradiated.

Considering surfaces diffuse, gray and with the emission negligence, Eq. (5) boundary is:

$$I_w = q_0 \frac{1}{4\pi}(1 - R_e) + \frac{R}{\pi}\int_{\hat{n}\cdot\hat{s}<0} I_i(\Omega_i)|\hat{n}\cdot\hat{s}|d\Omega_i \quad (7)$$

$\hat{n}$ and $\hat{s}$ are vectors: the first is outward normal to the surface and the second is a unit vector (same direction of I_i); in such a way that $\hat{n}\cdot\hat{s} = cos(\theta_i)$; θ_i is relative to normal surface and varies with z. Eq. (8) calculates the radiative flux, arriving from all directions, that crosses an area element (normal to z):

$$q_{r,z} = \int_{\Omega=0}^{4\pi} I(\Omega)cos(\theta)d\Omega \quad (8)$$

On the simulations is assumed that the reflectivity of surfaces of the slab are, externally, $R_e = 0$, *i.e.*, all radiative incident energy is absorbed to the inners surfaces of the slab and, internally, are $R = 1$ (left and right).

2.2 Tissue and nanoparticles properties

Following they are presented tissues properties and equations to obtain radiative properties of nanoparticles considered in this work.

Nanoparticles can be used to increase the absorption of incident radiation. To obtain these values for tissue layers with embedded gold nanoshells, was utilized the procedure proposed by Dombrovsky et al. (2011) on the following equations:

$$k_{sc} = k_t + 0.75 f_v \frac{Q_{abs}}{r} \quad (9)$$

$$\sigma_{sc} = \sigma_{sc,t} + 0.75 f_v \frac{Q_{sca}}{r} \quad (10)$$

Q_{abs} and Q_{sca} are absorption and scattering efficient factor, respectively, for a single particle; f_v is the volume fraction; k_t and $\sigma_{sc,t}$ are absorption and scattering to tissue layers without nanoparticles and r is nanoparticle radius.

To estimate the values of the efficiency factors (absorption and scattering), Dombrovsky et al. (2011) used Mie Theory to obtain; $Q_{abs} = 7.828$ and $Q_{sca} = 1.144$.

They utilized that's assumptions in this calculus: (1) The system are irradiated by a helium–neon laser with wavelength of 0.6328 μm; (2) Dimensions (maximum absorption to this wavelength) of silica-gold nanoshells (Fig. 1): *r=10 nm* (shell radius) and *0.725r* (silica radius); (3) Refractive index is *n = 1.45* (relative values to human ambient tissues for the nanoparticles); (4) volume fraction: f_v=10^{-5}.

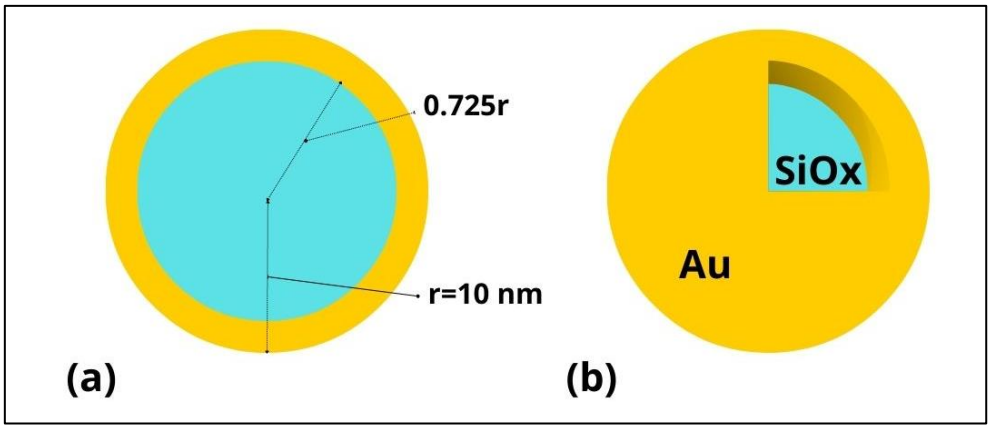

Figure 1. Representation of gold nanoshell. (a) Critical dimensions of nanoshell; (b) 3D form of nanoshell: silica kernel and gold spherical shell. Adapted from Lucena and Maurente (2021).

For this efficient factors values and f_v=10^{-5}, Eq. (9) and (10), provides to epidermis: $\kappa = 3115.6\ m^{-1}$ and $\sigma_{sc} = 1029\ m^{-1}$; tumor: $\kappa = 2985.5\ m^{-1}$ and $\sigma_{sc} = 1029\ m^{-1}$. Optical ($f_v$=0, *i.e.*, tissue without nanoparticles), and another physics properties of tissue layers are described on Table 1.

Table 1. Properties of tissues without nanoshells embedded.

Tissue Properties	Epidermis	Tumor	Papillary dermis	Reticular dermis	Fat
Density (kg/m^3)[(1)]	1200	1030	1200	1200	1000
Specific Heat (J/kgK) [(1)]	3589	3582	3300	3300	3674
Thermal Conductivity (W/mK) [(1)]	0.235	0.558	0.445	0.445	0.185
Heat Power (W/m^3) [(1)]	0	3680	368.1	368.1	368.3
Blood Perfusion Rate (kg/m^3) [(1)]	0	9.4	0.4	5.2	1
Absorption Coefficient (m^{-1}) [(1)]	180	50	20	20	10
Scattering Coefficient (m^{-1}) [(1)]	2360	600	200	200	400

[(1)] Data from Dombrovsky *et. al.* 2011. Adapted from Bruno *et. al.* 2017.

2.3 **Numerical Model**

To obtain the transient solution for the problem of coupled radiation, conduction and blood perfusion heat transfer, a Fortran90 code was developed. For the radiation heat transfer solution, a Monte Carlo Method, developed and employed by Maurente et al. (2007a, 2008b) and Maurente and França (2019), was improved to consider radiation scattering by tissues and nanoparticles, a while the Finite Volume method was employed to develop the code to solve the PBHE, accordingly the procedure presented by Maliska (1995). The algorithms can work with nonuniform meshes that simulated the comportment of nonhomogeneous biologic tissues and the temperature gradient gives PTT.

In Monte Carlo, radiation emission, propagation and absorption are stochastically modeled by emission, propagation, and absorption of Monte Carlo photons. In these simulations photons are emitted from the left boundary in Fig. 1, simulating radiation from the laser entering tissue. In order to minimize statistical oscillations, a total of 10^6 were released in each simulation.

2.4 **Studied Case**

The studied case was based on that approached by Dombrovsky et al. (2011). It consists of a one-dimensional slab of tissue with the five layers presented in Fig. 2., which comprises epidermis, tumor, papillary dermis, reticular dermis and Fat. Dombrovsky et al. (2011) assumed that nanoparticles are uniformly distributed along the two first layers. However, this is not usually the case in real PTT conditions. Two common procedures to embed nanoparticles in tissues are by injecting them either directly in the tissue or in the blood flow, which cause them to accumulate in the tumor region because of its typical vascularization characteristics.

In order to investigate the effects of different nanoparticles distributions, in a case of skin cancer, on divergence of radiative heat flux and temperature spatiotemporal profile, two cases were approached and comparted to that considered by Dombrovsky et al. (2011) of uniform distribution. These cases were based on results presented by Soni et al. (2014). They are: (1) Accumulation in the peripheral region of the tumor, 20% in each side of the tumor, leaving the meddle empty of particles (as depicted in Figure 2.c); (2) accumulation in the epidermis and first half of tumor (as depicted in Figure 2.d). Case (1) represents what occurs when particles are introduced via blood, while case (2) regards to injection directly in the tumor.

For all cases, the slab is irradiated, on the left, by a helium-neon laser with Emissive Power of 20 kW/m^2, during a time of 10 *s*. The laser radiation wavelength is 0.6328 μm. For the conduction analyses,boundaries conditions are: temperature of 37 °*C* at the left surface and; convective heat transfer to deeper regions of the tissue at the right boundary, being the; convective heat transfer coefficient equal to h=50 $W/(m^2K)$ and fluid temperature equal to 37 °*C*.

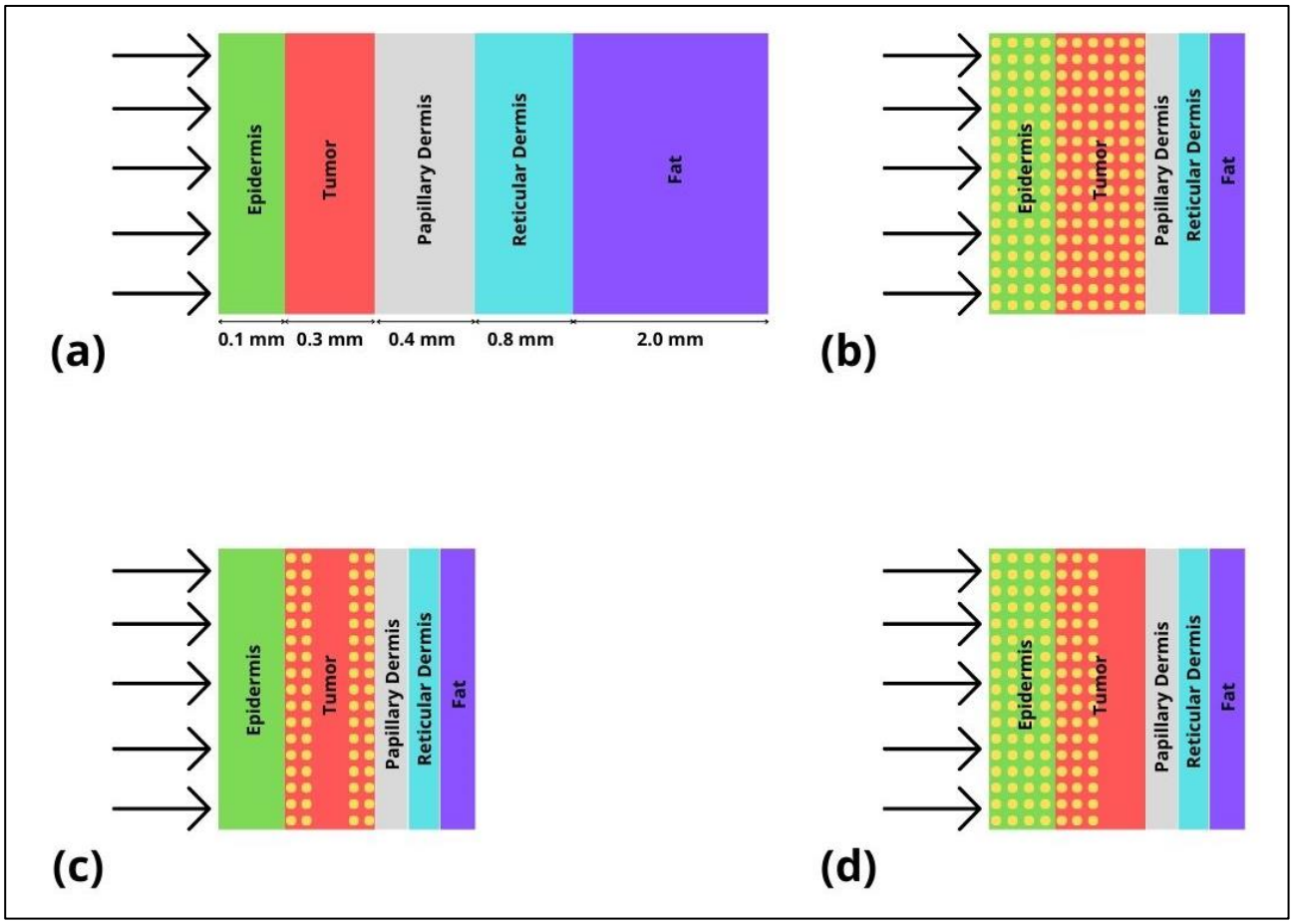

Figure 2. Representation of laser ablation the skin cancer. (a) Tissue layers (b) Standard case: nanoshells distributed on epidermis and tumor; (c) Case 1: nanoshells distributed on tumor's periphery; (d) Case 2: nanoshell distributed on epidermis and half of tumor.

3. RESULTS AND DISCUSSION

The results for case 1 and 2 are showed on this section. For each study carried out, the effects caused by the change in the position of the GNS (cases 1 and 2) in relation to the standard case were evaluated. They contemplate the spatial profile of heat flow divergence and temperature spatiotemporal profile in all tissues for each configuration.

In Figure 3, it is presented the divergence of heat flux from the solution of RTE, for all cases.

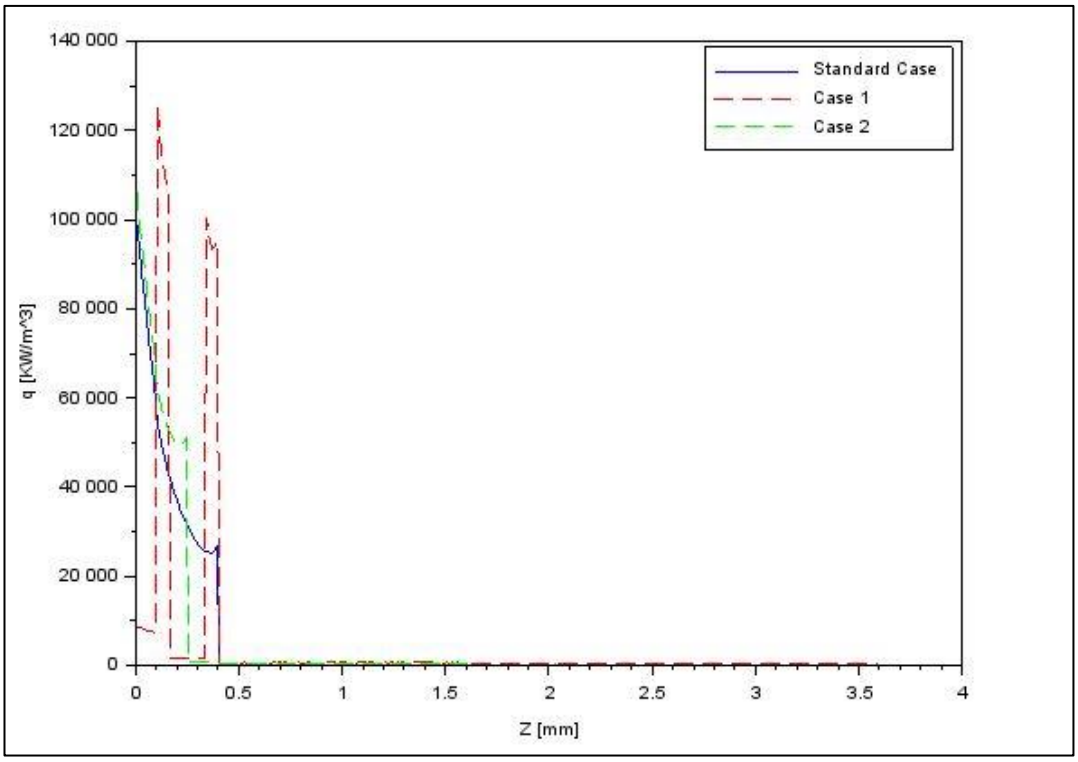

Figure 3. Divergence of heat flux.

The change in the spatial distribution of particles caused relevant changes in the peaks of the divergence radiative heat flux in terms of magnitude and location.

In case 1, the displacement of the particles to the peripheral region of the tumor (in relation to the standard case), not only changed the location, but also led to the emergence of a second peak, since particles concentrate into two regions: region 1 (0.1 to 0.2 mm) and region 2 (0.3 to 0.4 mm). The peak in region 2 is lower, it is located deeper inside the tissue as compared to the region 1 and thus receives less radiative energy. Another difference is that, in the standard case the peak occurred at the beginning of the epidermis, while in case 1 the absorption is higher in the edges of the tumor.

When particles are distributed only through the first half of the tumor (case 2), the abrupt decay of the divergence occurred earlier in relation to the standard case, beyond the region with nanoparticles, the divergence variation is less strong.

To investigate the influence of the nanoparticle's distribution on temperature. The divergences of the radiative heat flux presented in Figure 3 were used as a source terms for the PBHE solution. Results are presented in Figure 4.

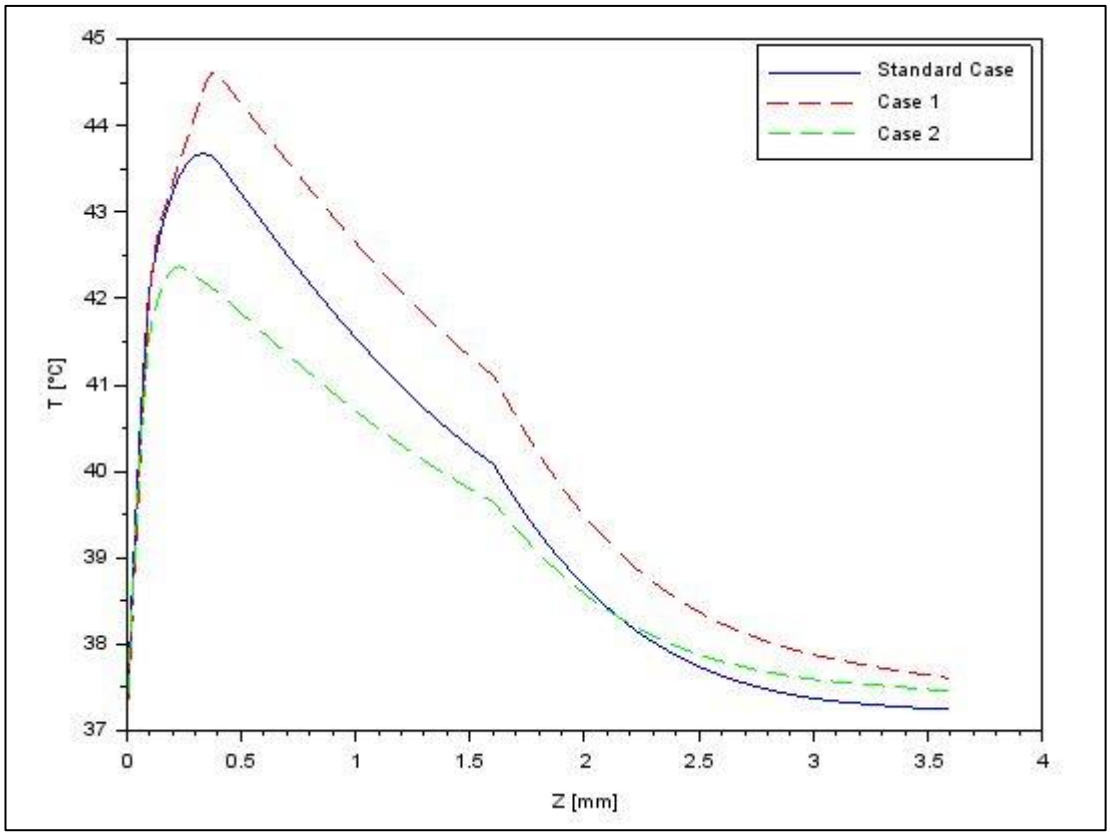

Figure 4. Temperature spatial profile after 10 s.

Changes in the GNS spatial distribution changes caused significant effects on the temperature.

By concentrating the nanoparticles in the peripheral region of the tumor, case 1; an increase in temperature was triggered in the tumor, but there was an increase in almost all healthy tissue compared to the standard case. The temperature peak was also change for the same cause; it's displaced for the final tumor session (about z=0.4 mm) with a positive temperature variation.

In case 2, there was a decrease in temperature throughout the cancerous region in relation to the standard case; The decrease of temperature from the GNS region to deeper tissue layers is relatively less accentuated as compared to the standard case. In the fat layer, the temperature becomes even higher than that of the standard case. It happens because the layer embedded with particles is thinner in case 2, allowing that a higher amount of the laser radiative energy penetrates to tissue regions behind the layer which has GNS. In other words, the radiative heat source is higher in deeper tissue regions in case 2 than in the standard case. In deeper regions of the tissue was relatively (about z=0.25 mm).

Fig. 5, show temperature variation with time into tumor critical locations:

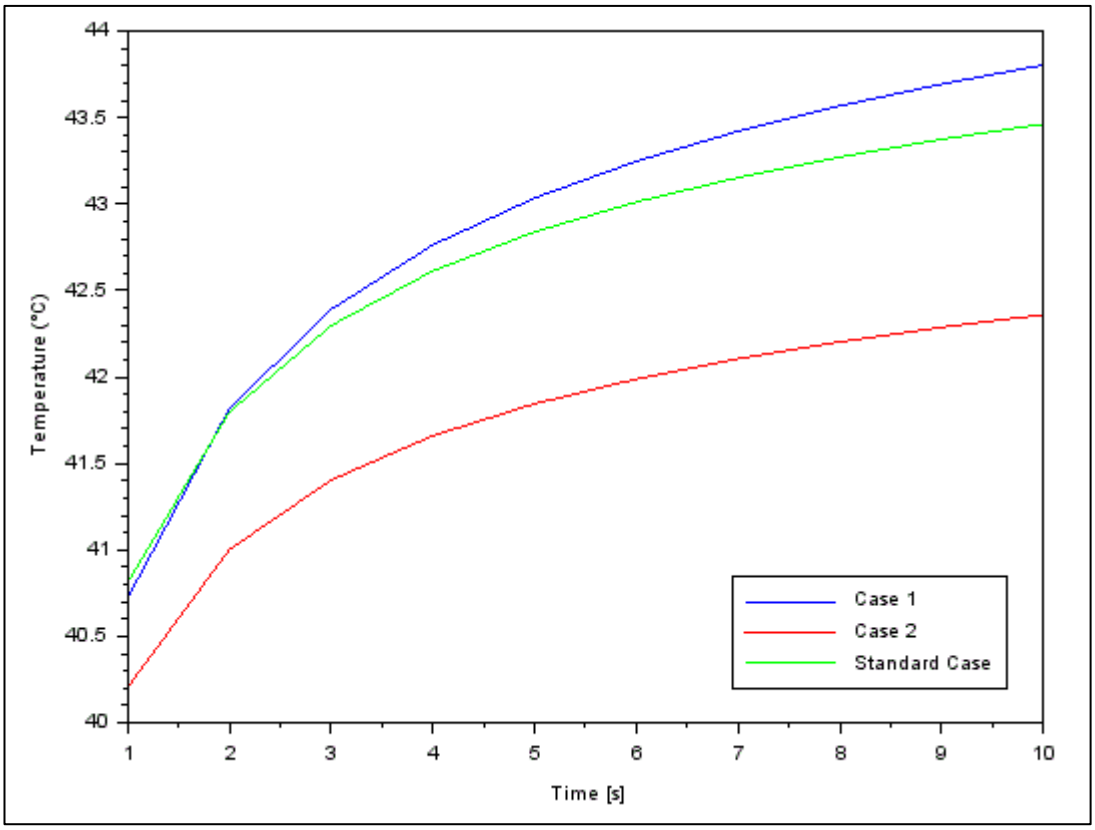

Figure 5. Temperature temporal profile on tumor (z=0.25 mm).

Figure 5 shows the variation of temperature with time in the middle of the tumor for the three considered cases, while Fig. 6 presents similar results to the tumor borders. As can be seen in these Figures, temperature rises faster in case 1 and slower in case 2.

A usual temperature assumed for hyperthermia is above 42 °C (42°C to 50°C) (Dombrovsky *et. al.* (2011)). As shown in Fig. 5, it takes about 2 s for the middle of the tumor reach this temperature in cases 1 and almost the same time interval in the standard case, while in case 2 the temperature reaches 42 °C only after 7 s of heating.

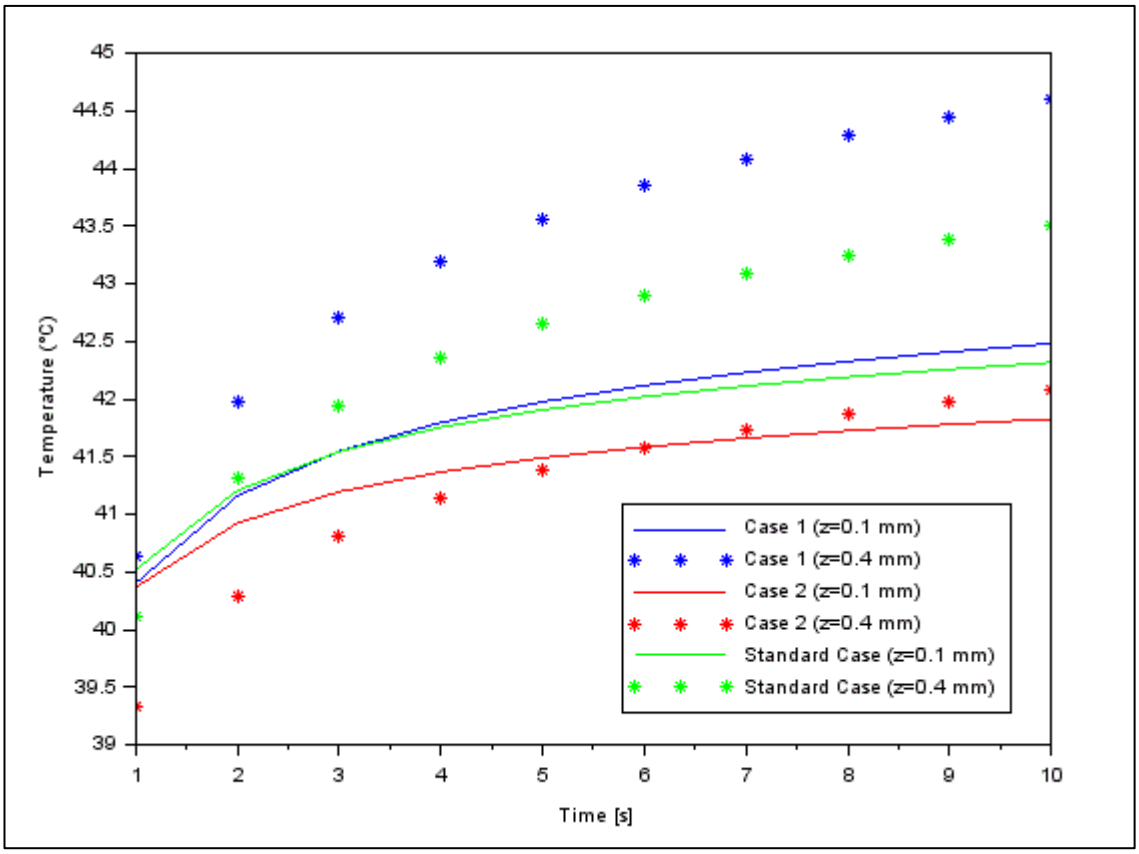

Figure 6. Temperature temporal profile on tumor's front (z=0.1 mm) and back (z=0.4 mm) extremities.

The goal in PTT is to make the cancerous cells to attain hyperthermia temperature and remain above such a temperature during a sufficient time to be killed, while keeping the temperature of the surrounding tissue as low as possible. In the considered cases, a manner of knowing whether the hyperthermia temperature was reached in any location of the tumor is evaluating the temperature of the tumor borders: front (z = 0.1 mm) and back (z = 0.4 mm).

In case 2, the temperature does not rise to 42 °C at front neither at back border, during all the 10s of heating, barely reaching this temperature only in the central region of the tumor.

In case 1 the hyperthermia temperature is attained along all the tumor about 5.5 s of heating and remains below 44.5 °C in any part of tissue outside the tumoral region.

In the standard case, hyperthermia temperature is reached at about 6.5 s and does not pass 43.5 °C at any location outside the tumor.

These results show that nanoparticles distribution significantly affect radiation absorption and temperature field. For example, in the hypothetical conditions considered in this work, the amount of energy delivered by the laser is not sufficient to induce hyperthermia in case 2. Thus, it would be necessary either higher laser power or longer heating time.

Differently, in the other two cases hyperthermia temperature is reached. However, the standard case of uniform distribution (Which is not guaranteed to happen in real cases) presents lower temperature at the back border and sharper decrease of temperature from the peak value, which is desirable in PTT.

4. CONCLUSIONS

Observing cases 1 and 2, it can be seen that particle distribution is a key parameter that directly affects temperature distribution. It can be clearly noticed that variations on distribution of nanoparticles causes strong changes in the heat flux divergence and, consequently, in the spatiotemporal profile of temperatures. Particles are deposited in tissues can change the conditions of hyperthermia (exposure time and temperature) throughout the tissue domain, *i.e.*, tumor and healthily zones.

Future studies can be carried out to investigate GNS configurations, *e.g.*, non-uniform volume fractions and particle concentrations in areas other than the central and peripheral regions of the tumor.

This study is important because it shows the importance of nanoparticles distribution, which varies with clinical protocols. Thus, it must be taken into account in future researches about PTT simulations.

5. ACKNOWLEDGEMENTS

L.I. wish to acknowledge the financial support provided by CAPES-Brazil for this research.

6. REFERENCES

BRUNO, Alexandre B. et al., 2017. Numerical simulation of nanoparticles assisted laser photothermal therapy: a comparison of the P1-approximation and discrete ordinate methods. *Journal of the Brazilian Society of Mechanical Sciences and Engineering*, Vol. 39, No. 2, pp. 621-630.

Dombrovsky, Leonid A. et al., 2011. "A combined transient thermal model for laser hyperthermia of tumors with embedded gold nanoshells". *International Journal of Heat and Mass Transfer*, Vol. 54, No. 25-26, pp. 5459–5469.

Ferlay, Jacques et al., 2021. "Cancer statistics for the year 2020: An overview". *International journal of cancer*, Vol. 149, No. 4, pp. 778–789.

Jain, Prashant K. et al., 2006 "Calculated absorption and scattering properties of gold nanoparticles of different size, shape, and composition: applications in biological imaging and biomedicine". *The journal of physical chemistry* B, Vol. 110, No. 14, pp. 7238–7248.

Januszewski, Adam; Stebbing, Justin, 2014. "Hyperthermia in cancer: is it coming of age?". *The lancet oncology*, Vol. 15, No. 6, pp. 565–566.

Kim, Donghyuk; Kang, Sukkyung; Kim, Hyunjung, 2021. "Numerical Study on Factors Affecting the Induction of Apoptotic Temperatures of Tumor in the Multi-Layer Skin Structure Using Monte Carlo Method". *Applied Sciences*, Vol. 11, No. 3, pp. 1103.

Kim, Minho; Lee, Jung-Hoon; Nam, Jwa-Min, 2019. "Plasmonic photothermal nanoparticles for biomedical applications". *Advanced Science*, Vol. 6, No. 17, pp. 1900471.

Lucena, Icaro; Maurente, Andre, 2021. "EFEITOS DA VARIAÇÃO DE PARÂMETROS FÍSICOS E ÓPTICOS NA TERAPIA FOTOTÉRMICA". Annals of IV SEMINÁRIO DO PROGRAMA DE PÓS-GRADUAÇÃO EM ENGENHARIA MECÂNICA - IV SEPEN. Natal, Brazil.

Maliska, C. R., 1995. *Transferência de Calor e Mecânica dos Fluídos computacional*. LTC, Rio de Janeiro. 1nd edition.

Maurente, André.; Vielmo, Horácio Antonio; França, Francis Henrique Ramos, 2007a. "A Monte Carlo implementation to solve radiation heat transfer in non-uniform media with spectrally dependent properties". *Journal of Quantitative Spectroscopy and Radiative Transfer*, Vol. 108, No. 2, pp. 295–307.

Maurente, André.; Vielmo, Horácio Antonio; França, Francis Henrique Ramos, 2008b. "Comparison of the standard weighted-sum-of-gray-gases with the absorption-line blackbody distribution function for the computation of radiative heat transfer in H2O/CO2 mixtures". *Journal of Quantitative Spectroscopy and Radiative Transfer*, Vol. 109, No. 10, pp. 1758–1770.

Maurente, André; França, Francis Henrique Ramos, 2015. "A Multi-Spectral Energy Bundle method for efficient Monte Carlo radiation heat transfer computations in participating media". *International Journal of Heat and Mass Transfer*, Vol. 90, pp. 351-357.

Modest, M., 2003. *Radiative Heat Transfer*. Elsevier, Amsterdã. 2nd edition.

Pennes, H.H, 1948. "Analysis of tissue and arterial blood temperatures in the resting human forearm". *Journal of Applied physiology*, Rockville. Vol. 1, No. 2, pp. 93–122.

Singh, Rupesh; Das, Koushik; Mishra, Subhash C, 2014. "Laser-induced hyperthermia of nanoshell mediated vascularized tissue–A numerical study". *Journal of thermal biology*, Vol. 44, pp. 55–62.

Soni, Sanjeev et al, 2014. "Investigation on nanoparticle distribution for thermal ablation of a tumour subjected to nanoparticle assisted thermal therapy". *Journal of thermal biology*, Vol. 43, pp. 70–80.

Soni, Sanjeev; Sinha, Ravindra K, 2016. "Controlling parameters for plasmonic photothermal ablation of a tumor". *IEEE Journal of Selected Topics in Quantum Electronics*, Vol. 22, No. 4, pp. 21–28.

Su, Di et al., 2010. "Multi-scale study of nanoparticle transport and deposition in tissues during an injection process". *Medical & biological engineering & computing*, Vol. 48, No. 9, pp. 853–863. transfer. Taylor & Francis Group, New York.

Vanderzee, Jill, 2002. "Heating the patient: a promising approach?". *Annals of oncology*, Vol. 13, No. 8, pp. 1173–1184.

7. RESPONSIBILITY NOTICE

The author(s) is (are) the only responsible for the printed material included in this paper.